Electronic Supplementary Material (ESI) for Soft Matter.
This journal is © The Royal Society of Chemistry 2018

Supplementary Information for "Clustering and assembly dynamics of a one-dimensional microphase former"

Yi Hu[a] and Patrick Charbonneau*[a,b]

[a] *Department of Chemistry, Duke University, Durham, North Carolina 27708, USA*
[b] *Department of Physics, Duke University, Durham, North Carolina 27708, USA*
* *Email: patrick.charbonneau@duke.edu*

February 13, 2018

1 Discretization choice in Transfer-matrix method

In the main text transfer matrices for the isothermal-isobaric ensemble are used to compute the system density and various other observables. For a fixed discretization scheme, the numerical error of this approach grows as temperature decreases or density increases. To analyze the main contributions to this error, we here investigate the results of computations under extreme conditions (for this article), $T = 0.2$ and $p = 0.01$ for $(\lambda, \kappa, \xi) = (2.5, 4, 1)$. Note that in this case, the thermodynamic density is $\rho = 0.60148(1)$.

1.1 Isometric Discretization

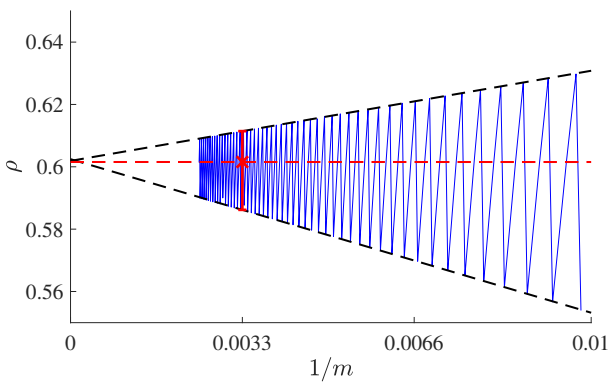

Figure S1: Convergence of the isometric discretization scheme with m. The asymptotic convergence in $1/m$ is accompanied by oscillations. Around $m = 300$, oscillations range $\sim 3\%$, but thanks to a fortuitous cancellation choosing $(m \mod 6) = 3$ (red dash line) reduces this error to a fraction of a percent. For $m = 303$, in particular, the error is 0.05%.

We first consider an isometric discretization of $s_i \in (1, \kappa)$. Figure S1 shows that density estimates for this scheme oscillate with discretization number m. The period corresponds to the number of bins needed to go from one integer subdivision of the attraction well to another. In the case of $(\lambda, \kappa) = (2.5, 4)$, $(m \mod 6) = 0$ sets the lower limit of the oscillation and $(m \mod 6) = 1$ it upper limit. The virial (main text, Eq. (15)) suggests that this behavior might

be related to the two discontinuities in the interaction potential: $r = 1$ and $r = \lambda$. Even though the transfer matrix includes third-nearest neighbor (3NN) interactions, these don't give rise to any discontinuity, hence only the NNN transfer matrix is here of interest.

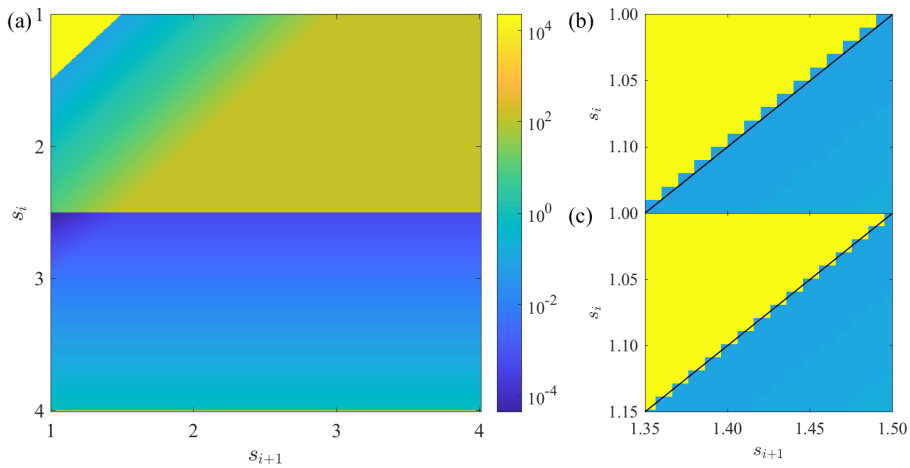

Figure S2: Transfer matrix for NNN interactions. (a) The whole matrix for $m = 300$; (b) Detail of (a) around the potential discontinuity at $s_i + s_{i+1} = \lambda$ (black solid line); (c) Detail of the same area for $m = 303$. Color encodes the magnitude of the entry on a logarithmic scale.

Visualizing the transfer matrix helps identify the numerical origin of this oscillation (Fig. S2). The main Boltzmann weights are found in the upper-left triangle of side $m/6$, which corresponds to next-nearest neighbor attraction regime. The hypotenuse coincides with the discontinuity of NNN interaction at $s_i + s_{i+1} = \lambda$. When $(m \mod 6) = 0$, the hypotenuse coincides with the right edge of the discontinuity for these entries (Fig. S2b). Because the fraction of entries that cross the discontinuity boundary is

$$\frac{2m/6}{(m+1)^2} \sim \frac{1}{m}, \tag{S1}$$

the error must asymptotically converge as $1/m$. As can be seen in Fig. S2c, a fortuitous cancellation surprisingly takes place for $(m \mod 6) = 3$. Optimizing this parameter is, however, not generally satisfying. More elaborate discretization schemes are necessary to reduce the error more systematically.

1.2 Simpson's Rule

To approximate the Boltzmann weight for an entry more precisely, an analogy to Simpson's rule for numerical integration is proposed:

$$\begin{aligned} M(s_i, s_{i+1}) &= \int_{s_i-\delta s/2}^{s_i+\delta s/2} \int_{s_{i+1}-\delta s/2}^{s_{i+1}+\delta s/2} e^{-\beta(u(s_1)+u(s_1+s_2)+ps_1)} ds_1 ds_2 \\ &= \frac{1}{36}\Big\{ e^{-\beta u(s_1-\delta s/2)-\beta p(s_1-\delta s/2)}(e^{-\beta u(s_1+s_2-\delta s)} + 4e^{-\beta u(s_1+s_2-\delta s/2)} + e^{-\beta u(s_1+s_2)}) \\ &+ 4e^{-\beta u(s_1)-\beta p s_1}(e^{-\beta u(s_1+s_2-\delta s/2)} + 4e^{-\beta u(s_1+s_2)} + e^{-\beta u(s_1+s_2+\delta s/2)}) \\ &+ e^{-\beta u(s_1+\delta s/2)-\beta p(s_1+\delta s/2)}(e^{-\beta u(s_1+s_2-\delta s)} + 4e^{-\beta u(s_1+s_2-\delta s/2)} + e^{-\beta u(s_1+s_2)})\Big\}, \end{aligned} \tag{S2}$$

where $\delta s_i = (\kappa - 1)/m$ denotes the interval of discretization. This general approach halves the oscillation strength compared to the midpoint rule (Fig. S3a).

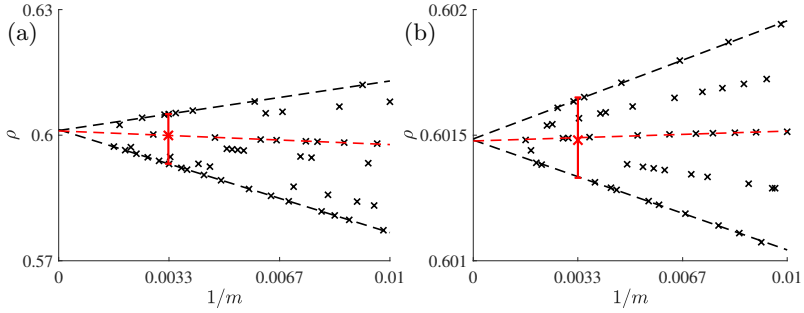

Figure S3: Density for different discretization schemes: (a) Simpson's rule and (b) two-part discretization. The results still converge as $1/m$, but now with a much smaller prefactor.

1.3 Two-part Discretization

Discretizing more finely the region of the matrix that contains the largest weights is also expected to improve the numerical accuracy. For the SWL model, this region corresponds to $s_i + s_{i+1} < \lambda$. For example, dividing the list of s_i into two parts $s_\mathrm{A} \in (1, s_\mathrm{d})$ and $s_\mathrm{B} \in (s_\mathrm{d}, \kappa)$, with $m = m_\mathrm{A} + m_\mathrm{B}$ and isometric discretization intervals $\delta s_\mathrm{A} < \delta s_\mathrm{B}$. Under the midpoint sampling rule, the error resulting from the discontinuity at $s_i + s_{i+1} = \lambda$ is reduced if m_A, δs_A and s_d satisfy

$$s_\mathrm{d} - 1 = m_\mathrm{A}\delta s_\mathrm{A} = \lambda - 2 + \delta s_\mathrm{A}/2. \tag{S3}$$

This choice minimizes the error because the division coincides with the discontinuity boundary regardless of m, as for $(m \mod 6) = 3$ in Fig. S2c. For $m = 300$, this two-part discretization gives $\rho = 0.60149$, which indistinguishable from the asymptotic value (Fig. S3b).

This scheme was implemented for the various calculations in this article. Because the choice ($T = 0.2$, $p = 0.01$) is an extreme case, we conclude that the result reported in this article have at most 0.1% error. This scale is smaller than the line width in the figures of the main text.

2 Correlation Length

The spatial correlation as a function of particle separation is defined as

$$G(i,j) = \langle (s_i - \langle s_i \rangle)(s_j - \langle s_j \rangle) \rangle = \langle s_i s_j \rangle - \langle s_i \rangle \langle s_j \rangle \tag{S4}$$

Generalizing the derivation described in Ref. 1, it can be shown that the correlation decays exponentially when $|i - j| \to \infty$. The correlation length is then $\xi_\mathrm{L} = \log(\Lambda_\mathrm{max}/|\Lambda_2|)^{-1}$, where Λ_2 is the second dominant eigenvalue of M.

In 1D SALR lattice models, the correlation length was found to display a marked growth at the onset of clustering.[2] Here, although the correlation length also grows with decreasing temperature at large ξ, its magnitude changes gradually and displays no remarkable feature around the onset of clustering. However, a separate peak does appear at small ξ, when the system undergoes condensation-like aggregation (Fig. S4). Here, the correlation length thus only captures ordering on length scales longer than that of the trimers.

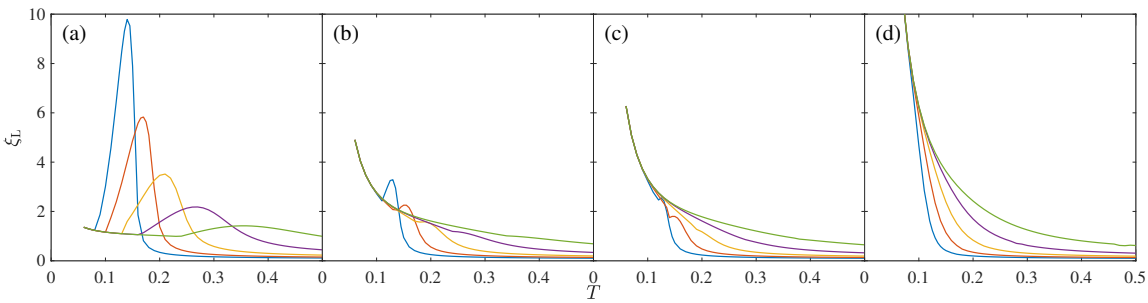

Figure S4: Correlation length, ξ_{L}, for different repulsion strength, (a)$\xi = 0.1$, (b)0.5, (c)0.6 and (d)1 for $\rho = 10^{-5}$ (blue), 10^{-4} (red), 10^{-3} (yellow), 10^{-2} (purple) and 10^{-1} (green) . Note that the λ transition identified by CDF is $\xi_\lambda = 0.51$.

3 Virial Coefficients Calculation

The second and third virial coefficients are obtained by integrating the Mayer function $f(r)$:

$$B_2(T) = -\frac{1}{2}\int f(r)dr, \tag{S5}$$

$$B_3(T) = -\frac{1}{3}\iint f(r)f(r')f(r-r')drdr', \tag{S6}$$

where

$$f(r) = e^{-\beta u(r)} - 1 = \begin{cases} -1, & r < 1, \\ e^{\beta} - 1, & 1 \le r < \lambda, \\ e^{-\beta\xi(\kappa - r)} - 1, & \lambda \le r < \kappa, \\ 0, & r \ge \kappa. \end{cases} \tag{S7}$$

The integral for $B_2(T)$ can be evaluated analytically

$$B_2(T) = -e^{-\beta(1-\lambda)} + \frac{1 - e^{-\beta\xi(\kappa-\lambda)}}{\beta\xi} + 2\lambda - \kappa. \tag{S8}$$

The analytical form of $B_3(T)$ is, however, somewhat more involved. It is here obtained by numerical integration (Fig. S5).

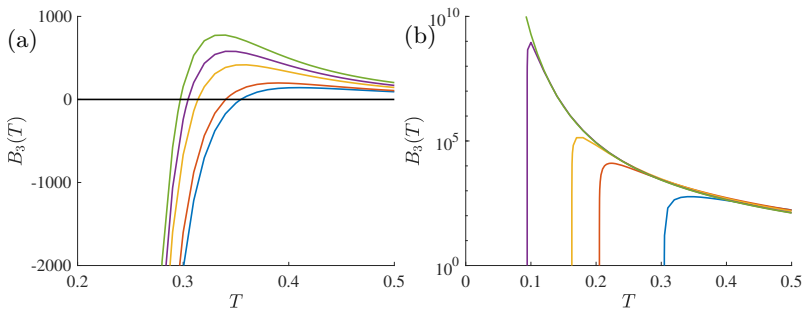

Figure S5: Third virial coefficient $B_3(T)$ under (a) $\lambda = 2.5$, where $\xi = 0, 0.1, 0.5, 1$ and 4, from bottom to top; (b) $\xi = 1$, where $\lambda = 2.5, 2.2, 2.1, 2.01$ and 2.0, from right to left.

The terminal clustering temperature T_{tc} can be estimated by solving $B_3(T_{\mathrm{tc}}) = 0$. For the 1D SWL potential $\kappa \le 4$ this condition has to be strictly followed for clustering to be possible; in

general higher-order coefficients can give rise to clustering even if $B_3(T) > 0$. Figure S5a shows that the zero of $B_3(T)$, when it exists, decreases with ξ, as illustrated in Fig. 6c of main text. This zero vanishes at $\lambda = 2$ (Fig. S5b).

References

[1] S. Varga, G. Ballo and P. Gurin, *J. Stat. Mech. Theory Exp.*, 2011, **2011**, P11006.

[2] J. Pękalski, A. Ciach and N. G. Almarza, *J. Chem. Phys.*, 2013, **138**, 144903.